Crystal growth and elastic properties of orthorhombic $Bi_2Ga_4O_9$

2006 J. Phys.: Condens. Matter 18 10977

(http://iopscience.iop.org/0953-8984/18/48/025)

INSTITUTE OF PHYSICS PUBLISHING JOURNAL OF PHYSICS: CONDENSED MATTER

J. Phys.: Condens. Matter **18** (2006) 10977–10988 doi:10.1088/0953-8984/18/48/025

Crystal growth and elastic properties of orthorhombic $Bi_2Ga_4O_9$

Jürgen Schreuer[1,4], Manfred Burianek[2], Manfred Mühlberg[2], Björn Winkler[1], Dan J Wilson[1] and Hartmut Schneider[3]

[1] Johann Wolfgang Goethe-Universität Frankfurt, Institute of Mineralogy/Crystallography, Senckenberganlage 30, D-60054 Frankfurt am Main, Germany
[2] Institute of Crystallography, University of Köln, Zülpicherstrasse 49b, D-50674 Köln, Germany
[3] Institute of Materials Research, German Aerospace Center (DLR), D-51174 Köln, Germany

E-mail: schreuer@ruhr-uni-bochum.de

Received 1 August 2006, in final form 11 October 2006
Published 17 November 2006
Online at stacks.iop.org/JPhysCM/18/10977

Abstract
The combination of favourable oxygen conductivity at high temperatures with mechanical strength make Bi-containing compounds with mullite-type crystal structures strong candidates for use as electrolytes of solid fuel cells. Large single crystals of orthorhombic $Bi_2Ga_4O_9$ with dimensions up to $20 \times 20 \times 10$ mm^3 were grown by the top-seeded solution growth technique. Their elastic constants at room temperature were determined for the first time using resonant ultrasound spectroscopy. The values given in GPa are $c_{11} = 143.4(2)$, $c_{22} = 161.7(2)$, $c_{33} = 224.2(3)$, $c_{44} = 69.6(1)$, $c_{55} = 49.2(1)$, $c_{66} = 76.5(2)$, $c_{12} = 73.7(2)$, $c_{13} = 62.2(3)$ and $c_{23} = 70.3(3)$. Further, the crystal structure and the elastic properties of $Bi_2Ga_4O_9$ were studied at 0 K by parameter-free *ab initio* calculations based on density-functional theory. On average the computed elastic constants differ from the experimental values by about 10%, indicating the reliability of the theoretical approach. Like in other mullite-type compounds the anisotropy of the longitudinal elastic stiffness is clearly controlled by the structurally dominant octahedral chains running parallel to [001]. The deviations from Cauchy relations show a significant anisotropy of the type $g_{22} > g_{11} \approx g_{33}$ which is related to the covalent character of the bonding interactions within the infinite ···–Bi–O–Bi–O–··· bond chains parallel to [010]. The mean elastic stiffness of $Bi_2Ga_4O_9$ is about 40% smaller than for 2/1-mullite and sillimanite. This discrepancy can be attributed to the mechanically very soft behaviour of the Bi $6s^2$ lone electron pair. Its stereochemical activity is clearly evident from both the asymmetry of the bismuth coordination polyhedron and the calculated electron density maps.

(Some figures in this article are in colour only in the electronic version)

[4] Author to whom any correspondence should be addressed. Current address: Ruhr-Universität Bochum, Institute of Geology, Mineralogy and Geophysics, D-44780, Bochum, Germany.

0953-8984/06/4810977+12$30.00

1. Introduction

Compounds of the composition $Bi_2M_4O_9$ ($M = Al^{3+}$, Ga^{3+}, Fe^{3+}, In^{3+}), $Bi_2Z_2M_2O_{10}$ ($Z = Mn^{4+}$, $M = Mn^{3+}$), their substituted derivates $Bi_{2-2x}A_{2x}M_4O_{9-x}$ (e.g. $A = Sr^{2+}$, $M = Al^{3+}$, Ga^{3+}, Fe^{3+}), and the wide field of respective mixed crystals belong to the family of mullite-type crystal structures [1]. This structure family is characterized by linear chains of edge-connected MO_6 octahedra, representing five single Einer-chains in a pseudo unit cell. The ideal arrangement of octahedral chains thereby occurs in space group $P4/mbm$. The mullite-type structure family allows a wide variation of polyhedra linking the backbone of the octahedral chains. In the $Bi_2M_4O_9$ group the octahedral chains are linked together by corner-connected MO_4 tetrahedra forming M_2O_7 dimers, and by highly asymmetric BiO_4 groups (see e.g. [2–8]). Between adjacent M_2O_7 dimers some of the possible oxygen positions remain unoccupied (figure 1) due to the stereochemical activity of the Bi $6s^2$ lone pairs which appear to point directly towards these vacant sites [7].

Like other bismuth phases, the mullite-type $Bi_2M_4O_9$ compounds are characterized by relatively high ion conductivities. In the case of $Bi_2Al_4O_9$ ceramics, values of approximately $10^{-2}\ \Omega^{-1}\ cm^{-1}$ at 800 °C have been reported [9]. The proposed mechanism of the oxygen ion conductivity is based on the sequence of alternating M_2O_7 dimers and oxygen vacancies along the [001] direction [7]. This structural arrangement allows, in principle, the migration of those oxygen atoms which connect the two tetrahedra of a dimer. The ion conductivity can be improved considerably if a proportion of the Bi^{3+} ions is replaced by divalent Sr^{2+}, and probably also by other cations like Eu^{2+} and Fe^{2+}. This leads to more complex compositions of the type $Bi_{2-2x}A_{2x}M_4O_{9-x}$ with $M = Al^{3+}$, Ga^{3+}, Fe^{3+} and $A = Sr^{2+}$, Eu^{2+}, Fe^{2+}. The electrical conductivity of ceramic $Bi_{1.8}Sr_{0.2}Al_4O_{8.9}$, for example, is approximately $0.28\ \Omega^{-1}\ cm^{-1}$ at 800 °C [9, 10].

The favourable oxygen conductivity values make the compounds strong candidates for use as electrolytes of solid oxide fuel cells (SOFCs). The electrolytes in SOFCs are subject to strong mechanical loads due to sudden temperature changes between room temperature and up to about 1000 °C. Therefore low thermal expansion coefficients, high thermal conductivities and suitable mechanical strengths and favourable elastic stiffnesses are required up to this temperature. It is the intention of this work to provide the first experimental data on the elastic constants of single-crystal $Bi_2Ga_4O_9$ and to discuss the structure-control of its elasticity in comparison to the behaviour of mullite *senso stricto* (mullite forms mixed crystals of the composition $Al_{4+2x}Si_{2-2x}O_{10-x}$, with $x = 0.25$ for stoichiometric mullite, i.e. so-called 3/2-mullite). In order to understand the role of the lone electron pair of bismuth, we performed model calculations of the crystal structure and the elastic properties based on quantum-mechanical methods. These discussions should help to elucidate the structure–property relationships and thus may further be used for the development of the material for potential SOFC applications.

2. Experimental details and results

2.1. Single-crystal growth

Dibismuth tetragallium oxide, $Bi_2Ga_4O_9$, is the only compound in the quasi-binary system Ga_2O_3–Bi_2O_3. A phase diagram of this system, given by Safronov *et al* [11] in 1971, shows that $Bi_2Ga_4O_9$ melts incongruently at about 1080 °C. Single crystals can be grown only from non-stoichiometric melts. The first attempts to grow $Bi_2Ga_4O_9$ from non-stoichiometric melts were carried out by Volkov and co-workers [12–14]. They reported crystal dimensions up to 12 mm on one side, but no information was given with respect to any crystalline quality.

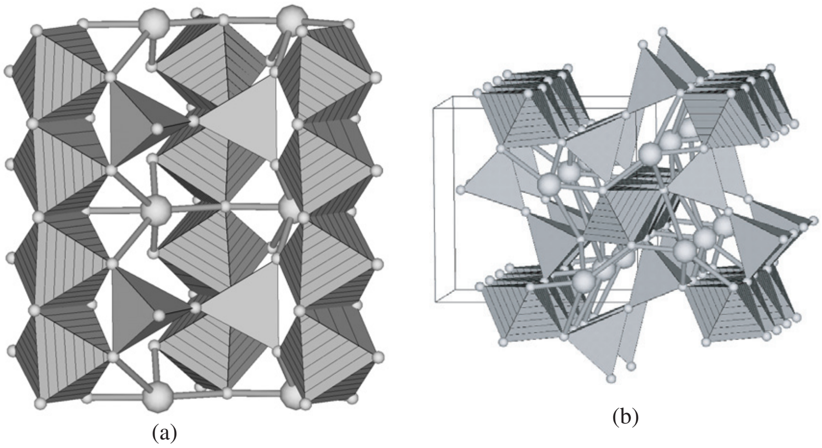

Figure 1. Projection of the crystal structure of $Bi_2M_4O_9$. (a) View parallel to the crystallographic a_1 axis, rotated by 5° around a_2 and 8° around a_3. (b) View almost parallel to [001] (from [1, 7]).

Table 1. Some experimental parameters of crystal growth of $Bi_2Ga_4O_9$ by the TSSG method.

Crucible dimensions	50 mm in diameter, 50 mm in height
Starting temperature	About 1025 °C, lowering down to 950 °C
Seed orientation	[001]
Cooling rate during growth	≈4 K/d
Cooling rate after growth	≈10 K/d

The phase diagram shows that the corresponding liquidus line is fixed at about 70 mol% Bi_2O_3 (peritectic point) and at about 90 mol% Bi_2O_3 (eutectic point). The eutectic temperature is about 735 °C. Such phase relations cause the ratio between the volume of the grown crystal and the inserted melt charge to be much less than unity. Hence, in the case of $Bi_2Ga_4O_9$ only 35% of the melt charge can be theoretically transferred into the single-crystalline state.

We have grown $Bi_2Ga_4O_9$ single crystals with dimensions up to $20\times20\times10$ cm^3 from non-stoichiometric melts by the top-seeded solution growth (TSSG) method. 4 N Ga_2O_3 (ChemPur GmbH, Germany) and single-crystal grade Bi_2O_3 (Heck GmbH, Germany) in a ratio of 1:3, and with a maximum weight of about 600 g, were inserted into a Pt crucible for synthesis at 1150 °C for about 72 h. A differential thermal analysis confirmed the incongruent melting behaviour at 1083 °C. The growth process is conducted in a tubular resistance furnace with a KANTHAL A1 heating system, and is monitored by weighing the crucible. Further details of the growth process are given in table 1.

A well-shaped and pale-yellow transparent $Bi_2Ga_4O_9$ single crystal is shown in figure 2. It possesses a symmetrical extinction between crossed polars in the visible part of the spectrum and is laterally surrounded by {110} faces. The top and bottom faces belong to the pinacoid {001}. Some regions of the crystal are clouded by inclusions of small solvent droplets.

2.2. Reference system and sample preparation

$Bi_2Ga_4O_9$ crystallizes in space group *Pbam* with lattice constants $a_1 = 7.929(1)$ Å, $a_2 = 8.295(1)$ Å and $a_3 = 5.893(1)$ Å, as determined by single-crystal x-ray diffraction using a Mach3 Enraf-Nonius four-circle diffractometer equipped with graphite-monochromatized

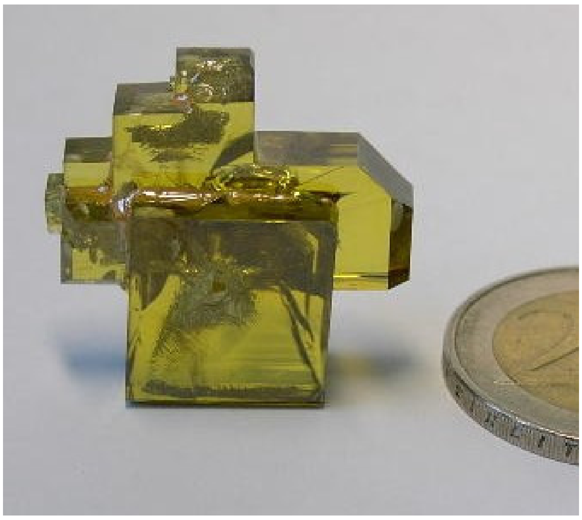

Figure 2. Multiple $Bi_2Ga_4O_9$ single crystal with dimensions of about $20 \times 20 \times 6$ mm^3. The morphology is dominated by the {001} pinacoid and {110} prism.

Mo Kα radiation. The elastic properties reported here are referred to a Cartesian reference system with axes $\mathbf{e}_i$ which are related to the crystallographic reference system by $\mathbf{e}_i \parallel \mathbf{a}_i$.

A rectangular parallelepiped suitable for resonant ultrasound spectroscopy (RUS) was cut from a large single crystal using a low-speed diamond saw and polished on diamond discs (mesh 1200). Orientation was controlled by Laue- and Bragg-diffraction techniques, with edges parallel to $\mathbf{a}_i$ and corresponding dimensions $l_1 \times l_2 \times l_3 = 3.990 \times 5.287 \times 6.025$ mm^3. Deviations from ideal orientation were less than 0.7° and opposite faces were parallel to within 2 μm. No defects such as inclusions and cracks could be seen with the naked eye. The geometrical density $\rho_G = M/l_1l_2l_3 = 7.189$ g cm^{-3} calculated from the sample dimensions and mass M agreed well with the density $\rho_B = 7.204(4)$ g cm^{-3} obtained by the buoyancy method on a large single crystal in pure water at room temperature. This indicates the high quality of the sample, particularly in respect to geometrical errors.

2.3. Resonant ultrasound spectroscopy (RUS)

The complete tensor of the elastic stiffnesses c_{ij} was determined at room temperature using an RUS system built in-house. The method is based on the measurement of ultrasonic resonance frequencies of a freely vibrating sample with well-defined shape. Particular advantages of RUS are (i) the possibility of deriving all independent elastic constants of a crystal species from a single sample with extraordinarily high internal consistency [15], (ii) the relatively small sample size compared to other ultrasound techniques, and (iii) no medium is required for transducer–sample coupling. Details on the RUS method can be found in the literature (see e.g. [16–18]).

Four resonance spectra of the rectangular parallelepipedal sample of $Bi_2Ga_4O_9$ were collected in the frequency range 200–1000 kHz, with the sample mounted in different orientations. The boundary conditions of a freely vibrating body were approached by touching the ultrasound transducers weakly to opposing corners of the sample. The mechanical loads were kept below 0.03 N. A total of 111 different resonance frequencies were extracted from the spectra and used in a nonlinear least-squares refinement that minimizes the quantity

$$\chi = \sum_{i=1}^{n} w_i (\omega_i^2(\text{calc}) - \omega_i^2(\text{obs}))^2$$

for n eigenfrequencies $f_i = \omega_i/2\pi$ by adjusting the elastic constants c_{ij} of the sample. The w_i are weights calculated from experimental errors of ±0.1 kHz in the determination of the resonance frequencies. The ω_i depend on sample orientation, shape and size as well as on mass density and elastic constants. In each cycle of refinement the eigenfrequencies of the sample were calculated by solving an eigenproblem, the rank of which equals the number of basis functions used. In order to minimize errors due to truncation effects, and due to the limited precision of floating-point numbers, 6900 normalized Legendre polynomials were used for the expansion of the components of the displacement vector. The convergence of the refinement procedure depends critically on the correct assignment of calculated to observed modes. Therefore, initial values of the longitudinal and transverse elastic stiffnesses c_{ii} were directly determined by applying the plate resonance technique (PRT) [19, 20] to the sample used for RUS measurements. The results in GPa are $c_{11} = 141(2)$, $c_{22} = 158(2)$, $c_{33} = 219(3)$, $c_{44} = 69.4(4)$, $c_{55} = 48.9(4)$ and $c_{66} = 76.8(4)$. The c_{ii} of $Bi_2Ga_4O_9$ are on average about 35% smaller than for 2/1-mullite [21]. Assuming the same mean ratio for the transverse interaction coefficients, we estimated initial values of c_{12}, c_{13} and c_{23} from the corresponding stiffnesses of 2/1-mullite. Using this set of parameters for the initial identification of the RUS modes, the refinement converged quickly. The final set of elastic constants yields an excellent match between calculated and experimental resonance frequencies, as indicated by a mean difference $\Delta f_i = |f_i(\text{calc}) - f_i(\text{obs})|$ of about 0.3 kHz and a maximum value of 1.25 kHz. Elastic constants obtained by the RUS technique are presented in table 2.

2.4. Quantum mechanical calculations

Our quantum mechanical calculations are based on density functional theory, DFT. While DFT itself is exact [24], actual calculations based on the Kohn–Sham formalism [25] require an approximation for the treatment of the exchange and correlation energies. Here we use the 'generalized gradient approximation', GGA [26]. Results based on GGA calculations are generally in better agreement with experiment than those obtained with the local density approximation, LDA [27–30].

Computationally efficient schemes in which the charge density and electronic wavefunctions are expanded in a basis set of plane waves are well suited to calculations of structure–property relations of compounds with the structural complexity of $Bi_2Ga_4O_9$. As it is impractical to consider tightly bound core electrons explicitly when using a plane wave basis set, pseudopotentials have to be used to mimic the screening of the Coulomb potential of the nucleus by the core electrons. A number of approaches for the construction of pseudopotentials have been presented in the literature [31, 32]. The state-of-the-art ones are the efficient 'ultrasoft' pseudopotentials, which require a comparatively small number of plane waves [33, 34]. Such ultrasoft pseudopotentials were used here, with a maximum cutoff energy of the plane waves of 380 eV. In addition to the cutoff energy, only one further parameter determines the quality of the calculations, namely the density of points with which the Brillouin zone is sampled. We used a sampling of reciprocal space such that distances between grid points are ≈0.03 $Å^{-1}$. All structural parameters not constrained by symmetry were relaxed simultaneously. After the final self-consistency cycle, the remaining forces on the atoms were less than 0.01 eV $Å^{-1}$, and the remaining pressure was less than 0.01 GPa. The present calculations are restricted to the athermal limit, in which temperature effects and

Table 2. Elastic constants of $Bi_2Ga_4O_9$ and structurally related compounds. ρ denotes the mass density, c_{ij} are elastic stiffnesses, B and C are bulk modulus and mean elastic stiffness, respectively, g_{ii} are the deviations from Cauchy relations and c_{ij}^{iso} are aggregate elastic constants calculated according to the Voigt–Reuss–Hill method. Methods: RUS (resonant ultrasound spectroscopy), BS (Brillouin spectroscopy), DFT-GGA (quantum mechanical calculations based on density functional theory in combination with the generalized gradient approximation).

Compound	$Bi_2Ga_4O_9$	$Bi_2Ga_4O_9$	2/1-mullite	Sillimanite	Sillimanite
Reference	This work	This work	[21]	[22]	[23]
Method	RUS	DFT-GGA	RUS	BS	DFT-GGA
ρ (g cm^{-3})	7.204		3.126	3.241	
c_{11} (GPa)	143.4(2)	163(3)	279.5	287.3	319
c_{22}	161.7(2)	161(9)	234.9	231.9	213
c_{33}	224.2(3)	199(2)	360.6	388.4	414
c_{44}	69.6(1)	62.8(5)	109.5	122.4	123
c_{55}	49.2(1)	36(6)	74.9	80.7	76
c_{66}	76.5(2)	68.1(5)	79.9	89.3	89
c_{12}	73.7(2)	86(2)	103.1	94.7	98
c_{13}	62.2(3)	68(2)	96.1	83.4	74
c_{23}	70.3(3)	75(2)	135.6	158.6	113
B (GPa)	101.9	109	166.5	167.1	159
C (GPa)	103.4	102	163.8	170.7	
g_{11} (GPa)	0.7	12.5	26.1	36.2	−10
g_{22}	13.0	32.2	21.2	2.7	−2
g_{33}	−2.8	17.7	23.2	5.4	9
c_{11}^{iso} (GPa)	181.4	177	284.8	295.2	294
c_{12}^{iso}	64.2	75	111.2	109.5	99

zero-point motions are neglected. The elastic stiffness coefficients have been obtained by the stress–strain method, where the c_{ij} are the proportionality constants linking the imposed strain and the resultant stress. Three strain patterns were imposed, in which for each strain patterns six distortions with a maximal amplitude of 0.003 have been employed. For the calculations we used academic and commercial versions of the CASTEP program, which has been described elsewhere [35–37].

The calculated elastic constants and structural parameters obtained from the geometry optimization are compared to experimental values in tables 2 and 3. The good agreement between the experimental and the theoretical values is typical for calculations such as those performed here. For example, in $Bi_2Ga_4O_9$, the Al_2SiO_5 modifications and spodumene the elastic constants calculated by DFT-GGA in the athermal limit deviate from the experimental ones obtained at room temperature on average by about ±10% (figure 3).

3. Discussion

As in sillimanite and 2/1-mullite, the anisotropy of the elastic properties of $Bi_2Ga_4O_9$ is clearly controlled by the structurally dominant composite chains running parallel to [001] (cf figure 1). In these compounds the backbones of the chains consist of edge-sharing MO_6 octahedra (M = Al, Ga). The free tips of adjacent octahedra are connected by TO_4 tetrahedra (T = Si, Al, Ga) and irregularly shaped BiO_4 polyhedra, respectively, which prevent any tilt of the octahedra. Consequently, the elastic behaviour of mullite and structurally related compounds is

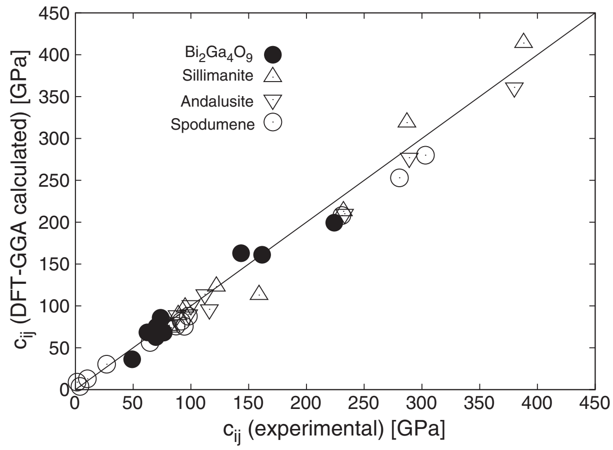

Figure 3. Comparison between experimental and calculated elastic constants of $Bi_2Ga_4O_9$, sillimanite [22, 23], andalusite [22, 23] and spodumene [38, 39].

Table 3. Comparison of experimentally determined and calculated structural parameters.

Reference		Exp. [4]	DFT This work
a_1 (Å)		7.934	8.012
a_2		8.301	8.473
a_3		5.903	6.030
Bi	x	0.174	0.1796
Bi	y	0.329	0.3216
Ga1	z	0.259	0.2585
Ga2	x	0.352	0.3532
Ga2	y	0.163	0.1633
O1	x	0.144	0.1527
O1	y	0.073	0.0619
O2	x	0.131	0.1334
O2	y	0.095	0.0906
O3	x	0.37	0.3769
O3	y	0.292	0.2891
O3	z	0.245	0.2419

qualitatively very similar (figure 4). The directions of the maximum of the longitudinal elastic stiffness, $c'_{1111}(\mathbf{u}) = u_{1i}u_{1j}u_{1k}u_{1l}c_{ijkl}$ (u_{1i} are direction cosines), coincide with the directions of the chains, whereas in the plane perpendicular to the chains c'_{1111} is about 35% smaller, showing only a weak anisotropy.

Hints at the nature of bonding interactions in crystals can be obtained by the deviations from Cauchy relations [40] represented by the second-rank tensor invariant $\{g_{mn}\}$ of the elasticity tensor with the components $g_{mn} = e_{mik}e_{njl}c_{ijkl}/2$, where e_{ijk} denote the components of the Levi-Civitá symbol. The longitudinal effect $g'_{11}(\mathbf{u}) = u_{1i}u_{1j}g_{ij}$ is closely related to the predominant bonding type in the plane normal to $\mathbf{u} = u_{1i}\mathbf{e}_i$. In ionic crystals, particularly in those built up from aspherical ions and constituents with large polarizability, the transverse interaction coefficients usually dominate over the corresponding shear stiffnesses, leading to positive deviations from Cauchy relations. Strong covalent or other bonds with preferred

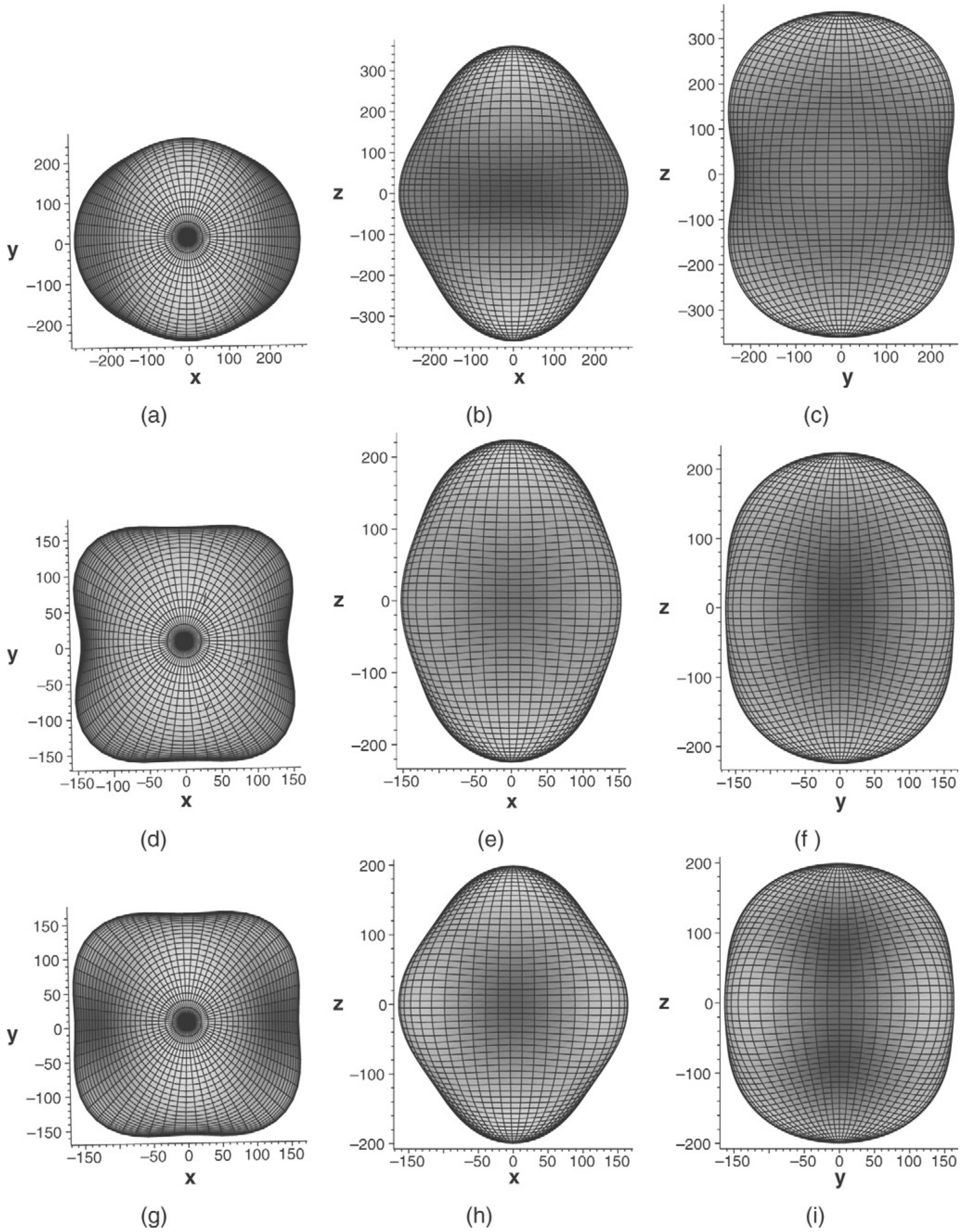

Figure 4. Surface of longitudinal elastic stiffness $c'_{1111} = u_{1i}u_{1j}u_{1k}u_{1l}c_{ijkl}$ (u_{1i} direction cosine) of 2/1-mullite [21] ((a)–(c)) and $Bi_2Ga_4O_9$ ((d)–(f) experimental results, (g)–(i) theoretical results). Each row shows views of the corresponding representation surface along [001], [010] and [100]. Larger and smaller values of c'_{1111} are indicated by darker and lighter colours, respectively. The labelling X, Y, Z of the axes correspond to the axes $\mathbf{e}_1$, $\mathbf{e}_2$ and $\mathbf{e}_3$ of the Cartesian reference system. Units are GPa.

bonding directions cause opposite effects. In 2/1-mullite the three-dimensional framework of Al–O and Si–O bonds leads to a nearly isotropic behaviour of g'_{11} whereas the deviations

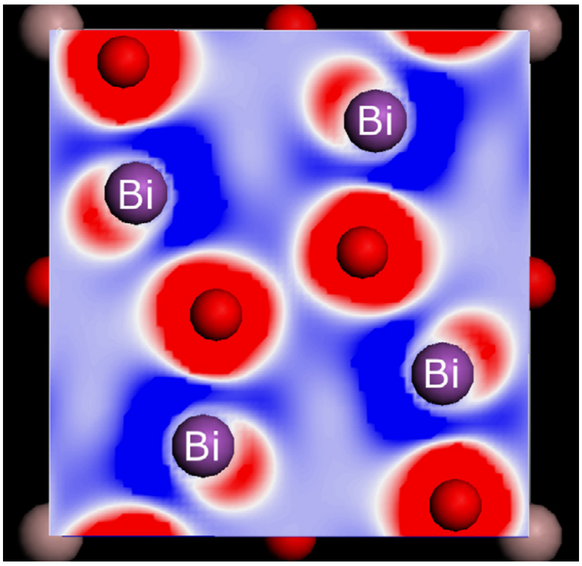

Figure 5. (001) slice at $z = 0$ of the calculated electron density difference map (a_1 horizontal, a_2 vertical). The localized lone electron pair is clearly visible as an umbrella-shaped charge accumulation about 0.75 Å from the Bi atom.

from Cauchy relations of $Bi_2Ga_4O_9$ are characterized by $g_{22} > g_{11} \approx g_{33}$ (table 2). This anisotropy indicates a dominance of directional bonding interactions within the principal bond chains of type $\cdots$–Bi–O–Bi–O–$\cdots$ running along [010] (cf figures 1(a) and 5), i.e. the Bi–O interaction is more covalent than the Ga–O bond.

The most remarkable differences in the elastic properties of mullite-type compounds investigated so far are found in the bulk modulus, B, and the mean elastic stiffness, $C = (c_{11} + c_{22} + c_{33} + c_{44} + c_{55} + c_{66} + c_{12} + c_{13} + c_{23})/9$, both scalar invariants of the elasticity tensor. The corresponding values for $Bi_2Ga_4O_9$ are about 39% smaller than for 2/1-mullite and sillimanite (table 2). This strong reduction cannot be simply explained by the substitution of Si and Al by Ga. For example, in the sequence $Y_3Al_5O_{12}$–$Y_3Ga_5O_{12}$ of mixed yttrium aluminium gallium garnets, C decreases only by about 10% with increasing amount of Ga [41]. Particularly useful for the further analysis of the mean elastic behaviour of $Bi_2Ga_4O_9$ is the quantity $S = CV_M$, defined as the product of the mean elastic stiffness and the molecular volume $V_M = M_W/(L\rho)$, with M_W the molar weight, L the Loschmidt or Avogadro number and ρ the mass density. In ionic crystals, the S-value can be decomposed into additive contributions $S(X_i)$ of stable constituents X_i of the compound X according to $S(X) = \sum S(X_i)$. The quasi-additivity of the S-values holds within 10% for a large variety of compounds, including halides, simple oxides, spinels, perovskites and most silicates [42, 43]. Applying this empirical rule we estimate $S(Bi_2O_3) = 382 \times 10^{-20}$ N m from the S-values of bismuth gallate, yttrium sesquioxide and yttrium gallium garnet, which is rather small in comparison to the corresponding values of group IIIa and IIIb sesquioxides (table 4). A similar observation has recently been made for bismuth triborate [44]. Haussühl *et al* attributed the soft elastic contribution of the bismuth component of BiB_3O_6 to the existence of a stereochemically active Bi $6s^2$ lone electron pair. Furthermore, the preferential orientation of the lone electron pairs parallel to the unique axis of this monoclinic crystal species leads to a pronounced minimum of the longitudinal elastic stiffness along the same direction. The elastic anisotropy

Table 4. Elastic S-values of selected oxides.

Compound	C (GPa)	ρ ($g\ cm^{-3}$)	S (10^{-20} N m)	Reference
$Bi_2Ga_4O_9$	103.4	7.204	2004	This work
$Y_3Al_5O_{12}$	186.3	4.55	4036	[41]
$Y_3Ga_5O_{12}$	167.7	5.79	3883	[41]
Y_2O_3	144.5	4.38	1237	[41]
Sc_2O_3	176.7	3.87	1045	[41]
B_2O_3			≈822	[44]
Al_2O_3 (corundum)	262.7	3.991	1114	[41]
Ga_2O_3			≈811	$(S(Y_3Ga_5O_{12} - 1.5 \cdot S(Y_2O_3))/2.5$
Bi_2O_3			≈382	$S(Bi_2Ga_4O_9) - 2 \cdot S(Ga_2O_3)$

as expressed by the ratio $c'_{1111}(\max)/c'_{1111}(\min) \approx 6.6$ is one of the largest reported for ionic crystals so far.

In $Bi_2Ga_4O_9$, both the geometry of the bismuth coordination polyhedron and the calculated electron density distribution give evidence for a stereochemically active lone electron pair. The crystal structure analyses [3, 4], as well as the Mulliken population analysis in the course of our quantum mechanical calculations, revealed that the Bi(III) is four-coordinated. These contacts, which are characterized by bond distances $d(\text{Bi–O}) < 2.439$ Å and bond populations of 0.28–0.08e, are essentially perpendicular to the chain axis, forming a highly asymmetric coordination shell. According to [45, 46] the vector

$$\Phi(X) = -\sum_{i=1}^{n} \exp(-d_i/g)\mathbf{u}_i$$

describes the stereochemical influence of a lone electron pair of an atom X with n ligands, where $\mathbf{u}_i$ is the unit vector pointing from the central atom to the ith ligand, d_i denotes the corresponding bond distance and $g = 0.2$ is an empirical constant. The length of Φ is a measure of the deviation of the spatial distribution of the lone electron pair from spherical symmetry. In the case of $Bi_2Ga_4O_9$, the experimental and theoretical values of $|\Phi(Bi^{3+})|$ vary between 2.1 and 4.1. Nevertheless, all values are within the range typical for a stereochemically active Bi $6s^2$ lone electron pair. The lone electron pair can also be easily identified in the calculated electron density difference maps obtained from our DFT-based calculations (figure 5). Contrary to the situation observed in bismuth triborate, the mutual orientation of neighbouring Bi lone electron pairs in $Bi_2Ga_4O_9$ is nearly perpendicular (figure 5), and the octahedral chains are linked in the (001) plane by a network of Ga_2O_7 dimers and Bi–O interactions. Thus, the anisotropies of the longitudinal elastic stiffness of $Bi_2Ga_4O_9$ and of other mullite-type compounds are qualitatively very similar.

4. Conclusions

In summary, we found that the contribution of the Bi_2O_3 component with a stereochemically active Bi $6s^2$ lone electron pair to the mean elastic stiffness of compounds containing bismuth sesquioxide is relatively small compared to those sesquioxides without lone electron pairs, e.g. Al_2O_3 and Ga_2O_3. This explains the small mean elastic stiffness of $Bi_2Ga_4O_9$ in comparison to 2/1-mullite. With respect to potential applications of $Bi_2Ga_4O_9$ in SOFCs we expect that substitution of Bi^{3+} by Sr^{2+} not only improves the ion conductivity of the material [9, 10] but also leads to a more favourable mechanical strength.

The observed depression of the mean elastic stiffness of $Bi_2Ga_4O_9$ is probably a general feature of compounds containing cations with lone electron pairs, e.g. Tl^+, Sn^{2+}, Pb^{2+}, As^{3+}, Sb^{3+} and Bi^{3+}. Moreover, preferential orientation of stereochemically active lone electron pairs can cause a pronounced elastic anisotropy. Therefore, we believe that elasticity would provide a highly sensitive probe for studying temperature- and pressure-induced changes in the stereoactivity of lone electron pairs.

Our promising results concerning the accuracy of elastic constant calculations are consistent with earlier findings. Although restricted to the athermal limit, our approach, based on DFT-GGA in combination with the 'imposed strain' method, allows one to predict reliable elastic constants of small crystal structures, like that of $Bi_2Ga_4O_9$, at pressures not accessible by experiment.

Acknowledgment

DJW would like to thank the MaterialsGrid project (http://www.materialsgrid.org) for funding.

References

[1] Fischer R X and Schneider H 2005 The mullite-type family of crystal structures *Mullite* ed H Schneider and S Komarneni (Weinheim: Wiley–VCH) pp 1–140
[2] Niizeki N and Wachi M 1968 The crystal structures of $Bi_2Mn_4O_{10}$, $Bi_2Al_4O_9$ and $Bi_2Fe_4O_9$ *Z. Kristallogr.* **127** 173–87
[3] Tutov A G and Markin V N 1970 The x-ray structural analysis of the antiferromagnetic $Bi_2Fe_4O_9$ and the isotypical combinations $Bi_2Ga_4O_9$ and $Bi_2Al_4O_9$ *Izv. Akad. Nauk SSSR Neorg. Mater.* **6** 2014–7
[4] Müller-Buschbaum H and de Beaulieu D Ch 1978 Zur Besetzung von Oktaeder- und Tetraederpositionen in $Bi_2Ga_2Fe_2O_9$ *Z. Naturf.* B **33** 669–70
[5] Giaquinta D M and Zur Loye H C 1992 Synthesis and structure of $Bi_2Fe_2Mn_2O_{10}$ *J. Alloys Compounds* **184** 151–60
[6] Giaquinta D M, Papaefthymiou G C and zur Loye H C 1995 Structural and magnetic studies of $Bi_2Fe_{4-x}Ga_xO_9$ *J. Solid State Chem.* **114** 199–205
[7] Abrahams I, Bush A J, Hawkes G E and Nunes T 1999 Structure and oxide ion conductivity mechanism in $Bi_2Al_4O_9$ by combined x-ray and high-resolution neutron powder diffraction and 27Al solid state NMR *J. Solid State Chem.* **147** 631–6
[8] Nguyen N, Legrain M, Ducouret A and Raveau B 1999 Distribution of Mn^{3+} and Mn^{4+} species between octahedral and square pyramidal sites in $Bi_2Mn_4O_{10}$-type structure *J. Mater. Chem.* **9** 731–4
[9] Bloom I, Hash M C, Zebrowski J P, Myles K M and Krumpelt M 1992 Oxide-ion conductivity of bismuth aluminates *Sild State Ion.* **53–56** 739–47
[10] Zha S, Cheng J, Liu Y, Liu X and Meng G 2003 Electrical properties of pure and Sr-doped $Bi_2Al_4O_9$ ceramics *Solid State Ion.* **156** 197–200
[11] Safronov G M, Speranskaya E I, Batog V N and Mitkina G D 1971 *Zh. Neorg. Khim.* **16** 526 (in Russian)
[12] Volkov V V and Egorysheva A V 1995 Synthesis and growth of $Bi_2Al_4O_9$ self-activated scintillator crystals *Inorg. Mater.* **31** 463–5
[13] Volkov V V and Egorysheva A V 1996 Photoluminescence in fast-response $Bi_2Al_4O_9$ and $Bi_2Ga_4O_9$ oxide scintillators *Opt. Mater.* **5** 273–7
[14] Volkov V V, Egorysheva A V, Kargin Yu F, Solomonov V I, Mikhailov S G, Buzmakova S I, Shul'gin B V and Skorikov V M 1996 Synthesis and luminescent properties of $Bi_2Ga_4O_9$ single crystals *Inorg. Mater.* **32** 406–9
[15] Schreuer J 2002 Elastic and piezoelectric properties of $La_3Ga_5SiO_{14}$ and $La_3Ga_{5.5}Ta_{0.5}O_{14}$: an application of resonant ultrasound spectroscopy *IEEE Trans. Ultrason. Ferroelectr. Freq. Control* **49** 1474–9
[16] Leisure R G and Willis F A 1997 Resonant ultrasound spectroscopy *J. Phys.: Condens. Matter* **9** 6001–29
[17] Migliori A and Sarrao J L 1997 *Resonant Ultrasound Spectroscopy* (New York: Wiley)
[18] Schwarz R B and Vuorinen J F 2000 Resonant ultrasound spectroscopy: applications, current status and limitations *J. Alloys Compounds* **310** 243–50
[19] Haussühl S 1983 *Kristallphysik* (Weinheim: Verlag Physik–Verlag Chemie)

[20] Haussühl S 2001 Plate modes *Handbook of Elastic Properties of Solids, Liquids, and Gases* vol 1 *Dynamic Methods for Measuring the Elastic Properties of Solids* ed A G Every and W Sachse (San Diego, CA: Academic) pp 283–98

[21] Schreuer J, Hildmann B and Schneider H 2006 Elastic properties of mullite single crystals up to 1400 °C *J. Am. Ceram. Soc.* **89** 1624–31

[22] Vaughan M T and Weidner D J 1978 The relationship of elasticity and crystal structure in andalusite and sillimanite *Phys. Chem. Minerals* **3** 133–44

[23] Winkler B, Hytha M, Warren M C, Milman V, Gale J D and Schreuer J 2001 Calculation of the elastic constants of the Al_2SiO_5 polymorphs andalusite, sillimanite and kyanite *Z. Kristallogr.* **216** 67–70

[24] Hohenberg P and Kohn W 1964 Inhomogeneous electron gas *Phys. Rev.* **136** B864–71

[25] Kohn W and Sham L J 1965 Self-consistent equations including exchange and correlation effects *Phys. Rev.* A **140** 1133–8

[26] Perdew J P, Chevary J A, Vosko S H, Jackson K A, Pederson M R, Singh D J and Fiolhais C 1992 Atoms, molecules, solids and surfaces: Applications of the generalized gradient approximation for exchange and correlation *Phys. Rev.* B **46** 6671–87

[27] Leung T C, Chan C T and Harmon B N 1991 Ground-state properties of Fe, Co, Ni and their monoxides: results of the generalized gradient approximation *Phys. Rev.* B **44** 2923–7

[28] Hammer B, Jacobsen K W and Norskov J K 1993 Role of nonlocal exchange–correlation in activated adsorption *Phys. Rev. Lett.* **70** 3971–4

[29] Goniakowski J, Holender J M, Kantorovich L N, Gillan M J and White J A 1996 Influence of gradient corrections on the bulk and surface properties of TiO_2 and SnO_2 *Phys. Rev.* B **53** 957–60

[30] Hamann D R 1996 Generalized gradient theory for silica phase transitions *Phys. Rev. Lett.* **76** 660–3

[31] Bachelet G B, Hamann D R and Schlüter M 1982 Pseudopotentials that work: from H to Pu *Phys. Rev.* B **26** 4199–228

[32] Kleinman L and Bylander D M 1982 Efficacious form for model pseudopotentials *Phys. Rev. Lett.* **48** 1425–8

[33] Vanderbilt D 1990 Soft self-consistent pseudopotentials in a generalized eigenvalue formalism *Phys. Rev.* B **41** 7892–5

[34] Kresse G and Hafner J 1994 Norm-conserving and ultrasoft pseudopotentials for first-row and transition elements *J. Phys.: Condens. Matter* **6** 8245–57

[35] Payne M C, Teter M P, Allan D C, Arias T A and Johannopoulos J D 1992 Iterative minimisation techniques for *ab initio* total energy calculations—molecular dynamics and conjugate gradients *Rev. Mod. Phys.* **64** 1045–97

[36] Milman V, Winkler B, White J A, Pickard C J, Payne M C, Akhmatskaya E V and Nobes R H 2000 Electronic structure, properties, and phase stabilities of inorganic crystals: a pseudopotential plane-wave study *Int. J. Quant. Chem.* **77** 895–910

[37] Segall M D, Lindan P J D, Probert M J, Pickard C J, Hasnip P J, Clark S J and Payne M C 2002 First-principles simulation: ideas, illustrations and the CASTEP code *J. Phys.: Condens. Matter* **14** 2717–44

[38] Sondergeld P, Li B, Schreuer J and Carpenter M A 2006 Discontinuous evolution of single crystal elastic constants as a function of pressure through the $C2/c \leftrightarrow P2_1/c$ phase transition in spodumene, $LiAlSi_2O_6$ *J. Geophys. Res.* **111** B07202/1–14

[39] Schreuer J, Winkler B and Haussühl S 2006 Elastic properties of pyroxenes spodumene, diopside, chromdiopside and aegirine *Phys. Chem. Minerals* in preparation

[40] Haussühl S 1967 Die Abweichungen von den Cauchy-Relationen *Phys. Kondens. Mater.* **6** 181–92

[41] Every A G and McCurdy A K 1992 *Second and Higher Order Elastic Constants* (*Landolt-Börnstein New Series* Group III, vol 29a) (New York: Springer)

[42] Haussühl S 1993 Interpretation of elastic properties of ionic crystals. Validity of a quasi-additivity rule? *Z. Kristallogr.* **205** 215–34

[43] Schreuer J and Haussühl S 2005 Elastic and piezoelectric properties of minerals II. Structure–property relationships *EMU Notes Mineral.* **7** 173–98

[44] Haussühl S, Bohatý L and Becker P 2006 Piezoelectric and elastic properties of the nonlinear optical material bismuth triborate, BiB_3O_6 *Appl. Phys.* A **82** 495–502

[45] Wang X and Liebau F 1996 Influence of lone-pair electrons of cations on bond-valence parameters *Z. Kristallogr.* **211** 437–9

[46] Liebau F and Wang X 2005 Stoichiometric *versus* structural valence: conclusions drawn from a study of the influence of polyhedron distortion on bond valence sums *Z. Kristallogr.* **220** 589–91